RF DEFLECTOR DESIGN AND MEASUREMENTS FOR THE LONGITUDINAL AND TRANSVERSE PHASE SPACE CHARACTERIZATION AT SPARC

David Alesini[1], Luca Ficcadenti[2], Giampiero Di Pirro[1], Andrea Mostacci[1,2], Luigi Palumbo[1,2], Cristina Vaccarezza[1], James Rosenzweig[3]

1) INFN-LNF Via E. Fermi 40, I-00044 Frascati, Italy

2) Università degli Studi di Roma "La Sapienza", Dip. Energetica, Via A. Scarpa 14, 00161, Roma, Italy

3) UCLA Dept. of Physics and Astronomy 405 Hilgard Ave., Los Angeles, CA 90095

Abstract

The six dimensional beam phase space at the end of a photoinjector can be completely characterized by means of an RF deflector and a dispersive system. In the paper we summarize the main features of the use of an RF deflector to characterize the longitudinal and transverse phase space. In particular we show the simulation of the measurement done in the case of SPARC photoinjector. We also illustrate the design procedure followed to design the RF deflector for SPARC. It is a five cell structure operating on the π-mode at 2.856 GHz. Finally we report and discuss the measurements results on a full scale aluminum prototype.

PACS: 41.75.-i, 41.60.Cr (da confermare)

Keywords: High-brightness beams; Soft X-ray FEL

Corresponding author:
D. Alesini (da confermare)
E-mail: alesini@lnf.infn.it
Phone: +39 06 94032639
Fax +39 06 94032256
Address:
Laboratori Nazionali di Frascati
Via E. Fermi 40
I-00044 Frascati, (Italy)

Introduction

The main goals of the SPARC [1] injector project are the generation of a high brightness electron beam able to drive a self-amplified spontaneous free-electron laser (SASE-FEL) experiment in the green visible light and the development of an ultra-brillant beam photo-injector needed for the future SASE-FEL based X-ray sources.
The characterization of the longitudinal and transverse phase space of the beam at the end of the injector is a crucial point in order to verify and tune all the photoinjector performances. With the use of an RF deflector it is possible to measure the bunch length [2,3] and, adding a dispersive system, the longitudinal beam phase space. Similarly, since the longitudinal beam distribution can be projected along a transverse coordinate, the transverse emittance of each longitudinal bunch slice can be measured using the quadrupole scan technique [4-6].
In the first paragraph of the paper we shortly review the basics principles of the longitudinal and transverse beam phase space characterization using an RF deflector. In the second paragraph we show the simulation of the measurements in the case of the SPARC photoinjector. In particular we illustrate the longitudinal phase space measurement (par. 2.1) and the horizontal beam slice emittance measurement (par. 2.2). In the third paragraph we illustrate the procedure followed to design the RF deflector for SPARC (par 3.1 and 3.2) and the RF measurement results on a full scale aluminum prototype (par. 4). Finally, in the fifth paragraph, we briefly illustrate the RF deflector power feeding system that we are planning to use.

1 Longitudinal and transverse beam phase space characterization using an RF deflector

The effect of the RF deflector on a beam traveling along the z direction is sketched in Fig.1: the RF deflector voltage (the integrated transverse Lorenz force per unit charge) is null in the center of the bunch and gives a linear transverse deflection to the head and tail of bunch. After the deflector, at the position of the flag, the transverse kick (vertical, for example) results in a transverse displacement of the centroid of each bunch slice proportional to the slice longitudinal position with respect to the bunch center. If the bunch length is L_B, the vertical dimension of the bunch at the flag, neglecting the vertical beam emittance of the bunch, is given by:

$$y_B = \sqrt{\beta_{y\_defl}\beta_{y\_flag}}\,\sin(\Delta\Phi)\frac{V_T}{(E/e)}\sin(\omega_{RF}L_B/2c) \underset{\lambda_{RF}>>L_B}{\cong} \frac{\omega_{RF}L_B V_T\sqrt{\beta_{y\_defl}\beta_{y\_flag}}\,\sin(\Delta\Phi)}{2cE/e} \tag{1}$$

where β_{y_defl} and β_{y_flag} are the vertical β-functions at the deflector and flag position, respectively, $\Delta\Phi$ is the phase advance between the deflector and the flag, ω_{RF} is the angular frequency of the deflecting voltage, $V_\perp$ is the peak transverse voltage, and *E/e* is the beam energy in *eV* units. If we consider a simple drift space of length L between the deflector and the flag, the previous expression reduces to:

$$y_B = \frac{\omega_{RF}LL_B V_\perp}{2cE/e}. \tag{2}$$

Equations (1) and (2) show that the longitudinal bunch distribution can be measured by measuring the transverse bunch distribution after the deflector.
In the real case, the transverse distribution of the bunch at the flag position is the superposition between the deflected beam size and the vertical dimension of the bunch slices at the flag position (σ_y), as illustrated in Fig. 1. The resolution length (L_{res}) can be defined as the bunch length that gives, on the flag, a vertical spot exactly equal to σ_y. From the previous expressions it is easy to verify that:

$$L_{res} \cong \frac{cE/e\sqrt{\varepsilon_y}}{\omega_{RF}\sqrt{\beta_{y\_defl}}\sin(\Delta\Phi)V_T} \tag{3}$$

where ε_y is the transverse vertical emittance of the beam. In the case of a drift space this expression becomes:

$$L_{res} = \frac{\sigma_y cE/e}{\omega_{RF} LV_\perp} = \frac{cE/e\sqrt{\varepsilon_y \beta_{y\_flag}}}{\omega_{RF} LV_\perp} \tag{4}$$

A sketch of the complete longitudinal phase space measurement setup is shown in Fig. 2. In this scenario, the bunch is vertically deflected by the RF deflector and horizontally by a magnetic dipole. The dispersion properties of the dipole allow to completely characterize the energy distribution of each bunch slice reconstructing of the bunch longitudinal phase space. In this case the energy spread resolution is simply given by:

$$\left.\frac{\Delta E}{E}\right|_{res} = \frac{\sqrt{\varepsilon_x \beta_{x\_flag}}}{D_{flag}} \tag{5}$$

where ε_x , β_{x_flag} and D_{flag} are the horizontal emittance, the horizontal β-function and dispersion at the flag position.
With the deflector it is also possible to measure the horizonthal beam slice emittance: the deflecting voltage gives the correlation between the longitudinal slice position and the vertical coordinate and the horizontal emittance can be measured with the quadrupole scan technique. The conceptual scheme is reported in Fig. 3.

2 Simulation of the measurements for SPARC

The SPARC photo-injector layout, reported in Fig. 4, consists of:

a) 1.6 cell RF gun of the BNL/UCLA/SLAC type [7] operating at S-band with incorporated metallic photo-cathode (Cu or Mg) and generating a 6 MeV electron beam;
b) two accelerating sections of the SLAC type (S-band, traveling wave).

The beam parameter list at the end of the injector is reported in Table 1.
A detailed layout of the magnets and flags that we will use for the longitudinal and transverse phase space characterization is reported in Fig. 5.

The longitudinal beam profile will be measured using the RF deflectors and directly analyzing the image produced by the beam on the flag F0 while the complete longitudinal phase space will be reconstructed using the RF deflector in combination with the dipole magnet and analyzing the image produced by the beam on the flag F1.
Using the RF deflector the horizontal slice emittance can be measured either on the transfer lines or on the dogleg, at the flags F0 or F3, respectively.The first two quadrupoles after the linac sections, Q_T1 and Q_T2, are used, in this case, for the quadrupole scan.

2.1 Simulation results of the longitudinal phase space measurement

In the SPARC case using Eq. (4) it is possible to calculate the longitudinal resolution (L_{res}) as a function of the deflecting voltage V_T. The result is plotted in Fig. 6 assuming L=2 m and $\sigma_y = 30\mu m$ at the flag position. In the SPARC case since the rms bunch length is about 1 mm, a resolution length of the order of $100\mu m$ is sufficient. Therefore a deflecting voltage of 1 MV can be chosen as the required RF deflector voltage for SPARC.
A 1.5 10^4 particles beam obtained from PARMELA [8] simulation at the end of the SPARC LINAC section has been tracked with the ELEGANT [9] code along the SPARC transfer lines. The beam images obtained at the RF deflector location and at the flag location, F0, are shown in Fig. 7.
The results of the data analysis are shown in Fig 8 where the vertical profile of the beam at the flag with V_T=1 MV and the longitudinal distribution of the bunch are displayed. The value of σ_z as obtained by applying Eq. (2) and by the longitudinal analysis of the raw data obtained from ELEGANT tracking agree with an error smaller than 1%.
The images collected on the dogleg at the flag located in F1 show the complete reconstruction of the longitudinal phase space as shown in Fig. 9, where the time-energy (t,p) distribution is replicated in the transverse plane (y,x). The “reconstructed” longitudinal phase space is in very good agreement with the real one.

2.2 Transverse phase space

The measurement of the beam slice emittance in the horizontal plane can be done with the quadrupole scan looking at the beam size at the flag locations F0 or F3, where two different values of image resolution can be achieved for the minimum horizontal rms size reconstruction. The optic functions of the SPARC transfer lines and dogleg for the measurement setup of the horizontal emittance are reported in Fig. 10.
In Fig. 11 the beam horizontal slice emittance is reported together with the two simulated measurements at F0 (b) and F3 (c), respectively. In the two flags it is possible to achieve two different resolutions investigating a wide range of beam emittance values [10].

3 RF deflector design

The required transverse deflecting voltage V_T=1 MV can be, in principle, achieved by both traveling wave (TW) or standing wave (SW) structures. In our case the choice between the two solutions is related to the maximum available input power (2 MW as shown in par. 5), space (about 0.4 m) and RF pulse length ($\approx 5\mu s$). Scaling known deflecting TW structures [11] to the SPARC frequency (f_{RF}=2.856 GHz) it follows that, to achieve the required deflecting voltage, the length of the deflector have to be $\approx 0.4m$ with a total number of cells equal to about 12. As shown in detail in the next paragraphs the same voltage can be achieved with a single SW cavity of about 0.05 m long. To allow reaching better resolution and flexibility, also considering longitudinal compression experiments in the next phases of SPARC [1], it has been proposed to adopt a 5 cells SW structure operating on the π-mode. As shown in the next paragraphs, this structure allows reaching a maximum transverse deflecting voltage of more than 3 MV with low peak surface electric field. Moreover, since the power to feed the cavity can be split out from the SPARC RF gun klystron waveguide (see par. 5) by a 10 dB directional coupler (the circulator and the directional coupler itself preserve the klystron and the RF gun from the cavity reflected power). We will first address the two dimensional design of the structure (sec. 3.1), i.e. without including the coupler and tuning system which are separately discussed later (sec. 3.2).

3.1 Two dimension design and electromagnetic characterization

To illustrate the procedure followed to design the 5 cell RF deflector, let us start with the single cell design. The first deflecting mode in a pillbox cavity is the TM_{110} mode and the deflection is given by the B field [12] only. In a single cell with irises (sketched in Fig. 12) there is a transverse E field component that contributes to the total deflection (see Fig 13). The ratio between the electric and the magnetic deflection contributions is strongly dependent from the irises aperture and can be from 10% for small irises to 90% for big irises apertures.
To adapt the single cell to the SPARC requirements, the inner radius (a) has been chosen equal to the SPARC beam pipe radius (20 mm), the cell length (d) equal to $c/2f_{RF}$ (with c velocity of light) to synchronize the bunch passage and the π-mode deflecting field with the external radius (b) has been tuned to set up the resonant frequency at 2.856 GHz by using the electromagnetic (e.m.) codes MAFIA [13] and HFSS [14] ([1]). The iris thickness (t) has been chosen at a reasonable value of 9.5 mm, considering that it is not a critical dimension in term of power dissipation, frequency sensitivities and deflection efficiency. The single cell final dimensions, parameters and frequency sensitivities, are reported in Table 2 assuming copper material. We have defined the transverse shunt impedance by the formula:

$$R_T = \frac{\left| \int_0^L \left(cB_x + E_y \right) e^{j\omega_{RF} z/c} dz \right|}{2P} \tag{6}$$

where B_x and E_y are the magnetic and electric transverse field components (with the proper phase), L is the cavity length, P is the dissipated power in the cavity and ω_{RF} is the angular frequency.

1 In the single cell simulations it has been assumed a perfect magnetic boundary conditions on the iris planes.

The dispersion curves of the single cell (obtained by MAFIA) are reported in Fig. 14. The deflecting π-mode has the frequency equal to 2.856 GHz, while the nearest monopole and dipole modes are far away from the deflecting one.
Different deflecting structure parameters and related scaling laws are reported in Table 3 as a function of the number of cells n ([2]). These results have allowed choosing the number of cells for the SPARC deflecting structure. The choice has been done taking into account the following constraints:

a) the available space in the SPARC transfer line;
b) the available transverse deflecting voltage for a given input power;
c) the mode separation with different number of cells to avoid problems of mode overlapping;
d) the maximum acceptable surface peak electric field to avoid problems related to high field intensities, discharges and so on.

The 5-cell deflecting structure fulfills all of the stated requirements. In fact, it allows operating with a very low input power $P_{RF} \leq 2MW$ obtaining contemporary low peak surface electric field and resolution length of the order of $12\mu m$. These parameters permit measurement of the longitudinal beam profile with good accuracy, even considering the possibility of longitudinal compression factors up to 20. Moreover the operation at low input power ($P_{RF} \leq 2MW$) allows to simplify the power line design as discussed in par. 5.
The complete 2D geometry, without coupler and tuning system, of the 5-cell RF deflector has been studied by using both MAFIA and HFSS and is reported in Fig. 15. The final dimensions, parameters and frequency sensitivities are reported in Table 4. The radius of the cells has been slightly adjusted (especially those of the cells connected to the beam pipe) in order to obtain a B field flatness smaller than 2% ([3]) as shown in Fig. 16. Concerning this last point it is important to remark that:

1) in multi-cells structures with small irises apertures, since the deflection is given essentially by the magnetic field, the B field flatness implies the uniformity of the deflection given by each cell;
2) in case of a structure with bigger irises, the deflection is given by both the magnetic and the electric field. Assuming an infinite number of cells, the B field flatness implies, also in this case, the uniformity of the deflection given by each cell;
3) in case of few coupled cells with big irises, nevertheless, the B field flatness does not necessarily imply the uniformity of the deflection given by each cell. In principle, it is possible to find a configuration of the cells radius that make the transverse deflection uniform from cell to cell [15]. It is, nevertheless, easy, to verify that field configurations slightly different from this optimum one (with deflecting force not perfect uniform), give variations of the transverse shunt impedance (R_T) of few percent.

From these considerations and also because a uniform B field flatness from cell to cell implies equal dissipation in all the cells, it has been optimized the cell radius in order to simply obtain the B field flatness.

---

2 The scaling laws are empirical and have been obtained from the analysis of different simulation results.
3 The B field flatness can be estimated taking the maximum difference of the B field peaks in each cell normalized to the maximum B field value.

Concerning the frequency sensitivities with respect to the outer radius of each cell ([4]), reported in Table 4, it is possible to conclude that errors in the cells machining of the order on $\pm 10\,\mu m$ give resonance frequency errors of the order of ± 100 kHz that can be easily compensated by a proper tuning system as shown in the next paragraph.

3.2 3D design and characterization

The 3D simulations of the deflecting structure has been performed using HFSS and have been oriented to:

1) design the input coupler;
2) design the tuning system;
3) design the system to split the frequency of the 90 deg tilted polarity with respect to the working one.

The coupler has been inserted in the central cell in order to not excite the $4/5\,\pi$ mode that has the frequency nearest to the π mode and no field in the central cell itself (see Fig. 17). To reduce the coupler window dimensions and, therefore, the perturbation to the deflecting field on the central cell, the smaller dimension ($34\,mm$) of the standard S-band waveguide has been tapered to the dimension of 16 mm. The HFSS simulated structure is plotted in Fig. 18. We have simulated one quarter of the deflector with the proper boundary conditions. The dimensions of the coupler window (w) and of the central cell radius (b_0) have been tuned in order to obtain a coupling coefficient $\beta = 1$, a resonant frequency of the whole system equal to 2.856 GHz and to preserve a good B field flatness. This has been done by following two steps:

1) a single cell with coupler has been simulated, tuning the dimensions of the coupler window and cell radius to obtain a coupling coefficient $\beta = 5$ (five times the coupling coefficient that we would reach with the complete structure) and a cell resonant frequency equal to 2.856 GHz;

2) the complete structure has been simulated starting from the dimensions found in the previous case and adjusting the dimensions of the coupler cell, window and cells dimensions to obtain $\beta = 1$, f_{RF}=2.856 GHz and B field flatness.

After this optimization we have obtained the dimensions and the final structure parameters reported in Table 5. The reflection coefficient at the input port is plotted in Fig. 19.
A complete analysis has been performed in order to calculate the frequency separation between the working deflecting mode and the other modes. It is important to distinguish between the four deflecting TM_{110}-like modes with the same polarity of the working one and those related to the 90 deg tilted polarity. Concerning the first category, the nearest $4\pi/5$ mode at 2.860 GHz is not excited by the coupler and it can, therefore, perturb only marginally the deflecting field. The nearest mode with the same polarity that can be excited by the coupler is the $3\pi/5$ mode (reported in Fig. 17) whose frequency is about +20 MHz away from the working one. To prevent the excitation of the modes with the 90 deg tilted polarity, two longitudinal rods (of radius r=1.5 mm) crossing off-axis the cells have been inserted, as shown in Fig. 20. The resonance frequencies of such modes are shifted far enough from the operating mode frequency (even if, in principle, they are not excited by the

[4] The outer radius of each cell is the most critical dimension in term of sensitivity.

central coupler). The calculated frequency shift given by the rods is about +50 MHz while the working mode is practically unperturbed.
Finally, for the tuning system, we have proposed to use cylindrical tuner of r=5 mm that gives a sensitivity of about 500 kHz/mm on the resonant frequency of each cell. The possible machining errors can be therefore compensated by a penetration of the tuners of few mm.

4 PROTOTYPE MEASUREMENT RESULTS

A full scale aluminum prototype has been constructed and is shown in Fig. 21. The cells are joined by six rods. To probe the field in the structure we have also inserted four lateral small antennas coupled with the working mode and with the 90 deg tilted polarity. The details of the tuning system, coupling window and rods are reported in Fig. 21. The prototype has been constructed in order to:

1) measure the resonant frequency and input port coupling coefficient;
2) measure the e.m. field of the working mode by the bead pull technique [16];
3) completely characterize the other modes of the RF deflector in term of frequency and e.m. field.

4.1 Resonant frequency and input port coupling measurements

The reflection coefficient at the coupler input port after the tuning procedure is reported in Fig. 22. As expected, with the input coupler it is possible to excite only 3 of the 5 deflecting modes. The measured external quality factor of the working mode is $Q_{EXT} \cong 17000$, in agreement with the simulation results ([5]), while the measured unloaded quality factor Q_0 is about 6300 and is lower than that we expected with aluminum (Q_0=14000) because of the fact that the structure is simply assembled and not welded. Concerning the 90 deg. tilted polarity, in Fig. 23 it is reported the transmission coefficient between the two probes coupled with the working mode and that between the two probes coupled with the tilted polarity. As expected the tilted polarity has a frequency shift more than +50 MHz.

4.2 Bead-pull measurements results

The measurements of the field in the cavity have been done with the bead-pull technique. The complete measurement setup is shown in Fig. 24. The PC controls both the network analyzer Agilent N5230A (interfaced by a GPIB Ethernet device) and the control circuit of the steeping motor through Labview [17]. The nylon wire is kept straight by a 75 g weight.
Since the deflection is given by both the magnetic and the electric field, both components have to be measured for a correct characterization of the device. Two types of perturbing objects have been used to measure the B-E field components: a small dielectric (teflon) cylinder (Fig. 25 (a)) and a small metallic sphere (Fig. 25 (b)). With the first object we have measured the E field component only while, with the second one, both the B and E field components. The used formulas were:

[5] Especially if we consider that , in the aluminium prototype there are strong losses and the Q_0 is strongly perturbed.

$$dielectric: \quad \frac{\Delta f}{f_0} = \varepsilon_0 \frac{1-\varepsilon_r}{2+\varepsilon_r}\left(k_{Edz} \frac{|E_z|^2}{W} + k_{Ed\perp} \frac{|E_\perp|^2}{W} \right)$$

$$metallic: \quad \frac{\Delta f}{f_0} = -\varepsilon_0 \left(k_{Emz} \frac{|E_z|^2}{W} + k_{Em\perp} \frac{|E_\perp|^2}{W} \right) + \mu_0 \left(k_{Bmz} \frac{|B_z|^2}{W} + k_{Bm\perp} \frac{|B_\perp|^2}{W} \right) \tag{7}$$

where Δf is the resonant frequency variation with respect to the unperturbed frequency f_0 ([6]), W is the total energy stored in the cavity and k_E, and k_B are the form factors of the E or B field with the subscripts "m" or "d" indicating the dielectric and metallic objects and "z" or "⊥" indicating the longitudinal or the transverse components of the field. On axis we have that B_z=0 and E_z=0.
In order to extrapolate the transverse magnetic field components one can proceed by following these two different ways:

1) if one is interested to the measurements of the magnetic field profile and not to its absolute value, one can simply scale the result of the first measurement in order to subtract the contribution of the electric field from the second one. Looking, in fact, at the field profile components reported in Fig. 16 one can observe that the two central peaks of the electric field correspond to zero crossing of the magnetic field. Therefore it is straightforward to subtract the contribution of the electric field from the second measurement just scaling the first measurement results by making equal the peaks of the electric field. This type of measurements can be useful if we are interested, for example, on the B field flatness tuning only;

2) if one is interested to the measurement of the absolute value of the B field one has to calibrate the perturbing objects doing measurements on different modes on a simple geometry (es. pillbox cavity) and calculating the coefficients through the formulas (7).

To calibrate the perturbing objects we have used the pillbox cavity shown in Fig. 26. The used resonant modes were the TM_{110} mode (that has no E field component on axis) to calculate the k_{Bm} factor and the TE_{111} mode (that has no B field component on the center of the cavity) to calculate the k_{Ed} and k_{Em} factors.
It is possible, also, to calculate the total deflection given to the particles by integrating the longitudinal electric field component off-axis and by using the Panofky-Wenzel theorem [19]. To do this it is possible to use a small metallic needle (Fig 25 (c)), with a form factor k_{Emz} previously calibrated. To calibrate the needle we have used the TM_{010} mode of the pillbox cavity.
The final measurement results are summarized in Figs. 27-30. The results of the measurements using the metallic sphere and the dielectric cylinder are reported in Fig. 27, where the average curves calculated over 30 measurements are plotted; the B field profile is sketched as well (green curve) and it has been calculated by the subtraction of the previous

6 Instead of the $\Delta-$frequency one can measure the $\Delta-$phase ($\Delta\phi$) of the transmission coefficient between two ports coupled with the field in the cavity since it is related to the frequency variation trough the formula:

$$\tan \Delta\phi = \frac{\Delta f}{f_0} 2Q_L$$

where, Q_L is the loaded quality factor of the resonance [18].

measurements as discussed above. The maximum standard deviation of measurements were about $1 \cdot 10^{-7}$ in case of dielectric cylinder and $7 \cdot 10^{-7}$ in case of metallic cylinder ([7]).
In Fig. 28 there are plotted the B and E field components obtained calibrating the measurements with the form factor found with the pillbox. In the same figure there are plotted the simulation results obtained by MAFIA.
Finally, in Fig. 29, there are reported the measurement results obtained with a metallic needle on-axis and 5 mm off-axis ([8]). The longitudinal electric field component off-axis has been obtained by simply subtracting the two measurements since the transverse E and B field components (affecting the measurements of the longitudinal electric field off-axis) do not vary, to the first order, with the transverse coordinate. In Fig. 30 it is reported the longitudinal E field component obtained by calibrating the measurements with the form factor found with the pillbox. In the same figure there are plotted the simulation results obtained by MAFIA.

5 RF deflector power feeding system

The 2 MW input power needed to feed the structure can be split out from the first klystron waveguide feed with a 10 dB directional coupler, as illustrated in Fig. 31. The circulator and the directional coupler assure that every reflected power from the deflector does not interact with the power feeding the RF gun. Moreover the high power switch is included to allow the deflecting field to be completely turned off.
Because of the reduced power needed for the structure it is possible to simply employ a waveguide system with air-fill, thus reducing the costs of the entire power feed system.

6 Conclusions

In the first part of the paper we have discussed how we intend to completely characterize the longitudinal and transverse phase space at SPARC. The methods are based on the use of an RF deflector that allows measuring the bunch length and the complete longitudinal phase space by adding a dispersive system. Using the quadrupole scan technique the horizontal beam slice emittances can also be measured. The simulations made by the ELEGANT code have shown the feasibility of this diagnostic system.
In second part of the paper we have illustrated the RF deflector design procedure made by the use of the e.m. codes MAFIA and HFSS. The RF deflector proposed is a 5 cells SW structure working on the π-mode at 2.856 GHz and fed by a central coupler with $\beta = 1$. Since the transverse shunt impedance is $\approx 2.5 M\Omega$ and the maximum input power is 2 MW, it is possible to obtain a resolution length of the order of $12\,\mu m$. Two small longitudinal rods have been inserted to shift the resonant frequency of the 90 deg tilted polarity with respect to the working mode. In the last part of the paper we have discussed the measurement results made on an aluminum prototype of the deflector. By the bead pull technique we have measured the deflecting field on axis. A tuning procedure has been implemented in order to reach a field flatness of the order of few percents. External quality factor measurements have also been done showing good agreement with expectations.

---

[7] We define the average curves and the maximum standard deviation as follow:
a) we have plotted the 30 measurements with the same longitudinal coordinate;
b) for each longiludinal coordinate we have calculated an average value and a standard deviation;
c) we have defined the average curve as the ensemble of the average values and the maximum standard deviation as the maximum of the standard deviations previously calculated.

8 In the figure there are plotted the average curves calculated over 30 measurements. The standard deviation of the measurements is $3 \cdot 10^{-7}$ in the case of the off-axis measurement and $1 \cdot 10^{-7}$ in the on-axis case.

7 Acknowledgements

This work has been partially supported by the EU Commission in the sixth framework programme, contract no. 011935 EUROFEL-DS1.

5 REFERENCES

[1] Preliminary Technical Design Report for the SPARC Advanced Photo-Injector, www.lnf.infn.it, 2004.
[2] G.A. Loew and O. H Altenmueller, “Design and applications of RF deflecting structures at SLAC”, PUB-135, Aug. 1965.
[3] P. Emma, et al., “A Transverse RF deflecting structure for bunch length and phase space diagnostics”, LCLS-TN-00-12, 2000.
[4] D.H. Dowell et al, “Slice Emittance Measurements at the SLAC Gun Test Facility”, SLAC-PUB-9540, September 2002.
[5] J.F. Schmerge et al, “Transverse-emittance measurements on a S-band photocathode RF electron gun”, Nucl. Instr. & Meth. A 483, 2002, pp. 301-304.
[6] X. Qiu et al ,”Demonstration of Emittance Compensation through the Measurement of the Slice Emittance of a 10- ps Electron bunch”, Phys. Rev. Lett. 76, 20, 1996, pp. 3723-3726.
[7] D.T. Palmer, “The next generation photoinjector”, PhD. Thesis, Stanford University.
[8] J. Billen, “PARMELA”, LA-UR-96-1835, 1996.
[9] M. Borland, elegant: A Flexible SDDS-Compliant Code for Accelerator Simulation, LS-287, Argonne National Laboratories, April 2000.
[10] D. Alesini and C. Vaccarezza, “Longitudinal and transverse phase space characterization at SPARC”, SPARC note, 2003.
[11] P. Bernard and H. Lengeler, “On the design of disc-loaded waveguides for RF separators“, CERN 68-30, Geneva, 1968.
[12] R. E. Collin. Foundations for Microwave Engineering. McGraw-Hill Book Co., pp 504-508, New York, 1992.
[13] www.cst.de.
[14] www.ansoft.com.
[15] L. Ficcadenti. Caratterizzazione e ottimizzazione di una cavita deflettente a RF. Tesi di Laurea, A.A. 2003-2004, Università degli studi di Roma La Sapienza.
[16] L. C. Maier Jr. And J. C. Slater. Field Strenght Measurement in Resonant Cavities. Journal of applied phisycs, 23(1), August 1951.
[17] National Instruments LabVIEW, www.ni.com\labview.
[18] F. Casper, G. Dome. Precise perturbation measurements of resonator cavities and higher order mode identification. CERN SPS/85-46 (ARF), November 1985.
[19] G. Dome, “Basic RF theory, waveguides and cavities”, RF engineering for particle accelerators, CAS-Cern Accelerator School, CERN 92-03, Geneva, 1992.

Table 1: beam parameter list at the end of the SPARC injector.

Electron Beam energy [MeV]	155
Bunch charge [nC]	1.1
Repetition rate [Hz]	10
Cathode peak field [MV/m]	120
Photocathode spot size [mm]	1.13
Laser pulse duration [ps]	10
Bunch energy @ gun exit [MeV]	5.6
Bunch peak current @ linac exit [A]	100
RMS normalized transverse emittance @ linac exit [mm mrad]	<2
RMS slice normalized transv. emit. @ linac exit (300 μm) [mm mrad]	<1
RMS longitudinal emittance @ linac exit [deg keV]	1000
RMS energy spread [%]	0.2
RMS bunch length @ LINAC exit [mm]	1

Table 2: single cell dimensions, parameters and sensitivities.

Dimensions [mm]		Parameter	MAFIA results	HFSS results	Sensitivities (MAFIA results) $[kHz/\mu m]$	
a	20.00	f_{res} [GHz]	2.855925	2.855905	$\partial f_{res}/\partial a$	-19
b	60.01	Q_0	16250	15979	$\partial f_{res}/\partial b$	43
t	9.50	R_T $[M\Omega]$	0.49	0.49	$\partial f_{res}/\partial t$	1.4
d	52.48	R_T/Q $[M\Omega]$	30.4	30.9	$\partial f_{res}/\partial d$	1.8
		$E_{peak}/\sqrt{P}\left[V/mW^{-1/2}\right]$ (*)	$7.45\cdot10^4$	$6.92\cdot10^4$		

*maximum electric field on the surface.

Table 3: deflecting cavity properties as a function of the number of cells and scaling laws.

Number of cells	Total length cells $L \cong 0.0525 * n\,[m]$	Transverse Shunt Impedance $\boldsymbol{R_T \cong 0.5 * n}$ $[M\Omega]$	Nearest mode frequency separation $\Delta f \cong 116/n^2$ $[MHz]$	$E_{peak}/\sqrt{P} \cong 7.45\cdot10^4/\sqrt{n}$ $\left[V/mW^{-1/2}\right]$
3	0.16	1.5	13	$4.31\cdot10^4$
5	0.26	2.5	4.6	$3.34\cdot10^4$
9	0.47	4.5	1.4	$2.49\cdot10^4$

Table 4: 5-cells structure dimensions, parameters and sensitivities.

Dimensions [mm]		Parameters	HFSS	MAFIA	Sensitivities (MAFIA) $kHz/\mu m$	
b_0	60.04	f_{res} [GHz]	2.855961	2.855596	$\partial f_{res}/\partial b_0$	-9.6
b_1	59.93	Q_0	16540	16329	$\partial f_{res}/\partial b_1$	-10.5
b_2	60.72	$R_T\ [M\Omega]$	2.44	2.40	$\partial f_{res}/\partial b_2$	-8.1
a	20.00	$R_T/Q\ [M\Omega]$	148	147		
t	9.5	$E_{peak}/\sqrt{P}\ [V/mW^{-1/2}]$	$3.33\cdot10^4$	$3.40\cdot10^4$		
d	52.48					

Table 5: RF Deflector final dimensions and parameters obtained with HFSS.

Dimensions [mm]		Parameters	Driven solution	Eigenmode solution
b_0	60.04	f_{res} [GHz]	2.856152	2.856178
b_1	59.93	Q_0	15240	16312
b_2	60.72	$R_T\ [M\Omega]$	2.24	2.39
a	20.00	$R_T/Q\ [M\Omega]$	147	147
t	9.5	$E_{peak}/\sqrt{P}\ [V/mW^{-1/2}]$	$3.39\cdot10^4$	$3.35\cdot10^4$
l_w	16.0	β	1	/
w	19.0			
h	1.1			

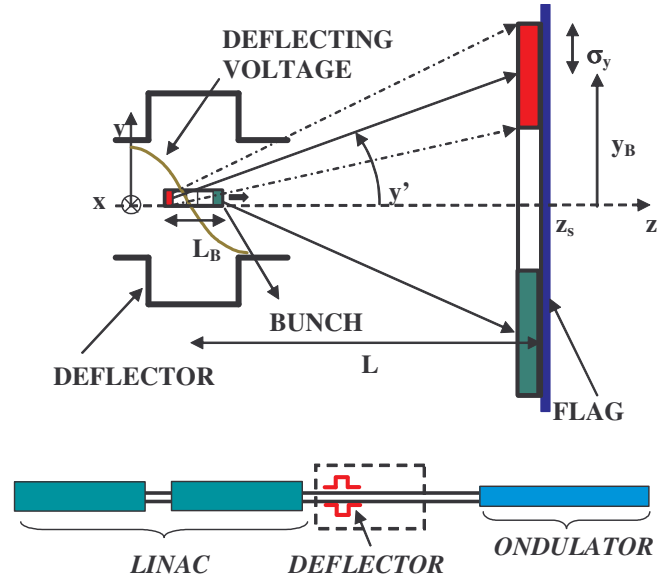

Fig. 1: Bunch length measurement schematic setup using an RF deflector.

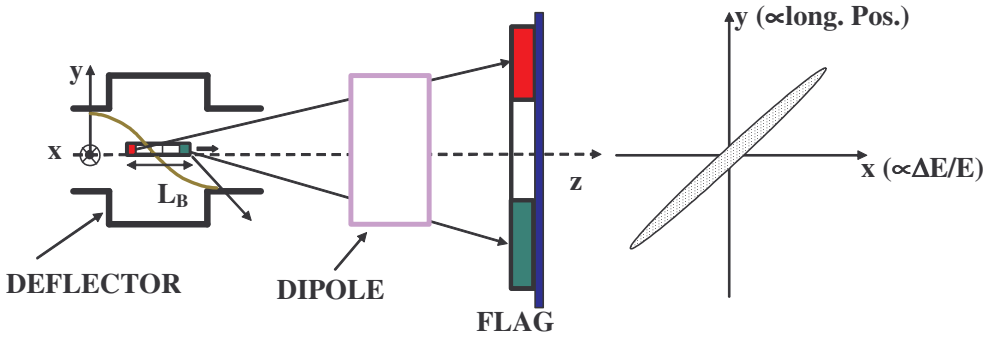

Fig. 2: Longitudinal phase space measurement setup using an RF deflector and a dipole magnet.

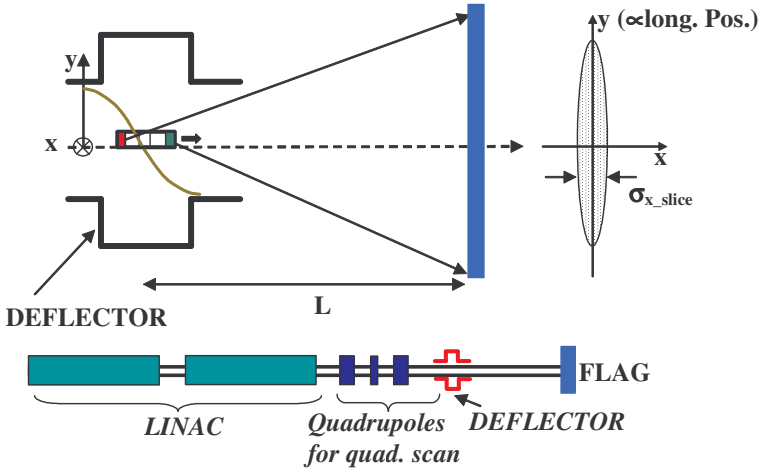

Fig. 3: Horizontal slice emittance measurement schematic setup using an RF deflector.

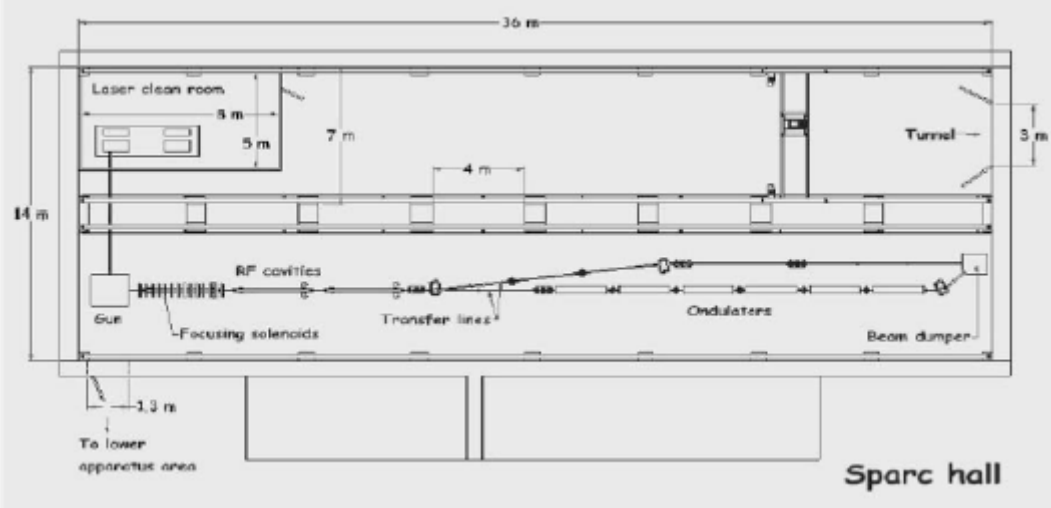

Fig. 4: SPARC photo-injector layout.

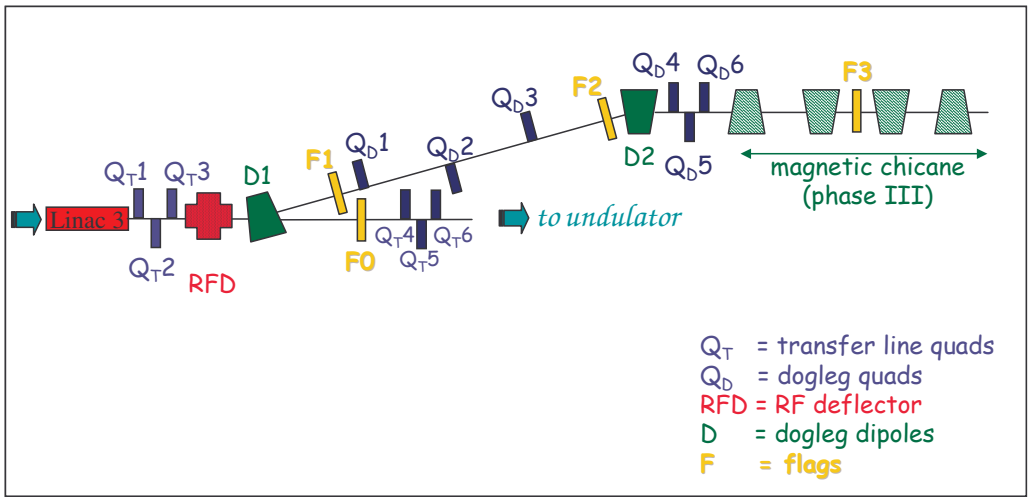

Fig. 5: Schematic layout of the magnets at the end of the SPARC photoinjector for longitudinal and transverse phase space characterization with an RF deflector.

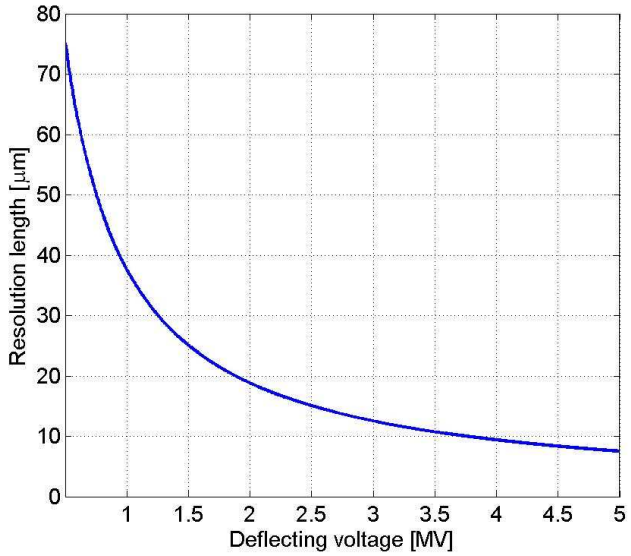

Fig. 6: Resolution length as a function of the deflecting voltage.

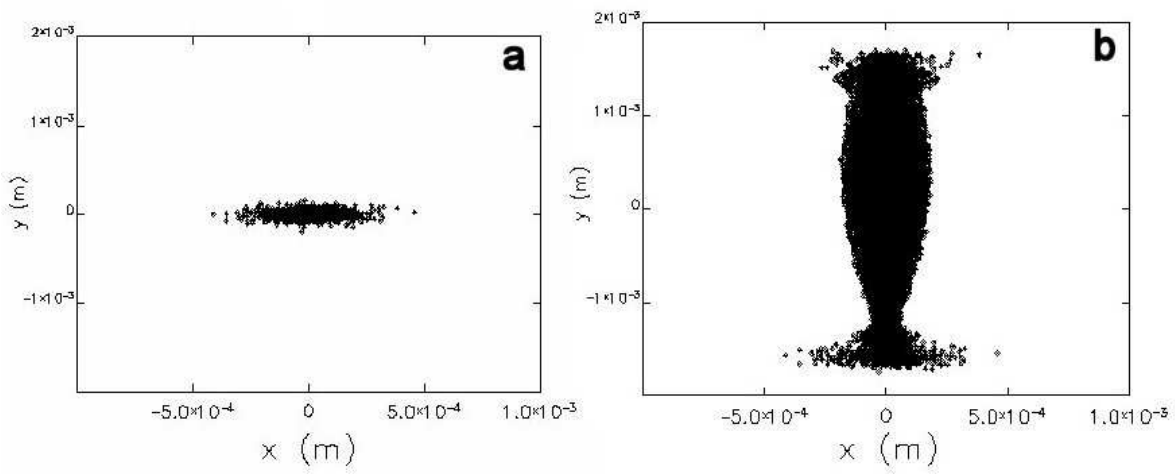

Fig. 7: (a) bunch transverse distribution at the RF deflector location; (b) bunch transverse distribution at the flag location.

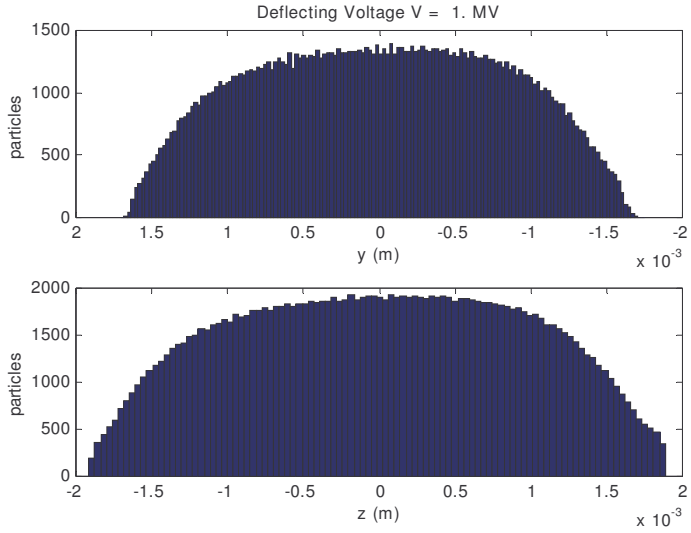

Fig. 8: Above: the longitudinal bunch distribution as projected by the RF deflector on the vertical coordinate of the flag F0; below: the same bunch longitudinal distribution vs. longitudinal coordineta (z-axis).

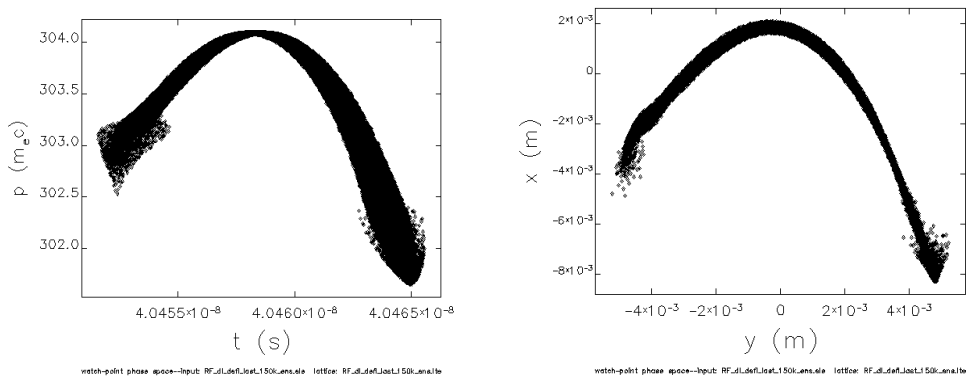

Fig. 9: (a) bunch longitudinal phase space at F1; (b) bunch transverse distribution at F1 after deflection.

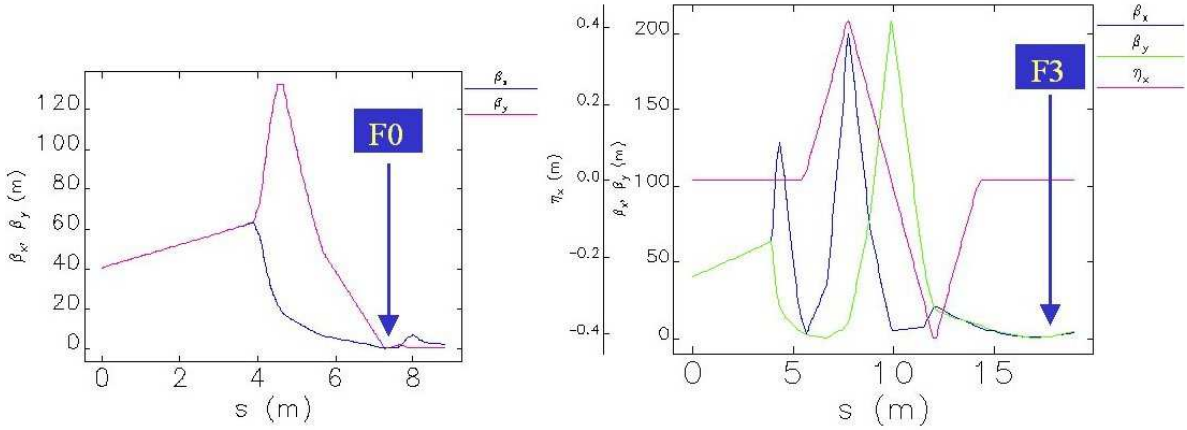

Fig. 10: SPARC transfer lines optic functions for the horizontal quad scan at F0 (left) and F3 (right). The origin of the longitudinal coordinate corresponds to the exit of the second linac section.

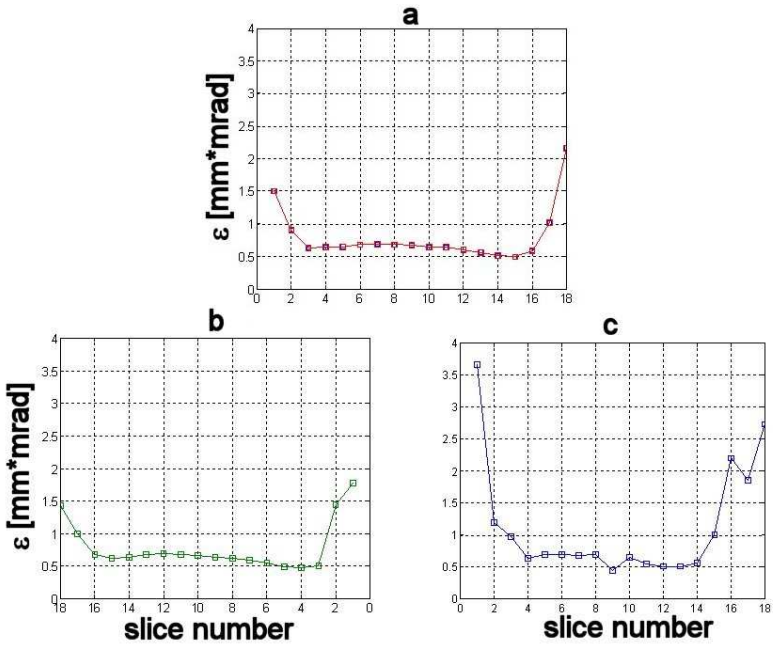

Fig. 11: (a) horizontal beam slice emittance as a function of slice number; (b), (c) reconstructed horizontal beam slice emittance by quadrupole scan at the flag F0 and F3 respectively.

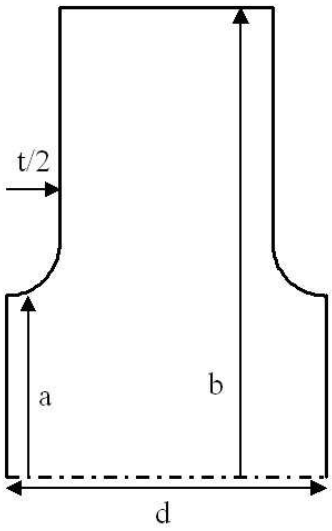

Fig. 12: Single cell of the RF deflector.

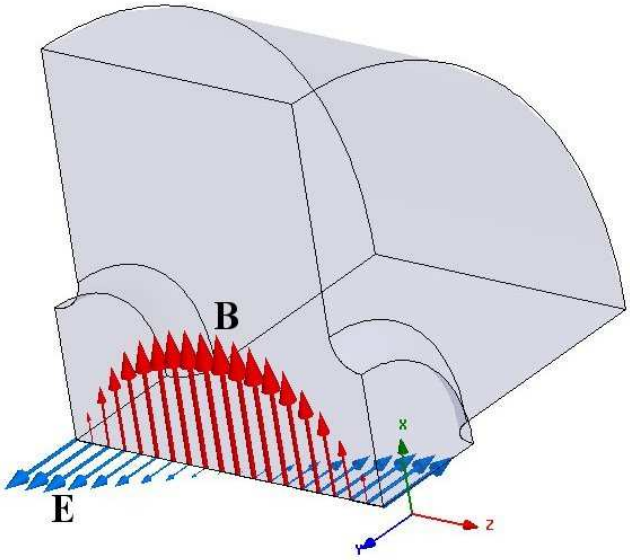

Fig. 13: Field profiles of the deflecting mode TM_{110}-like.

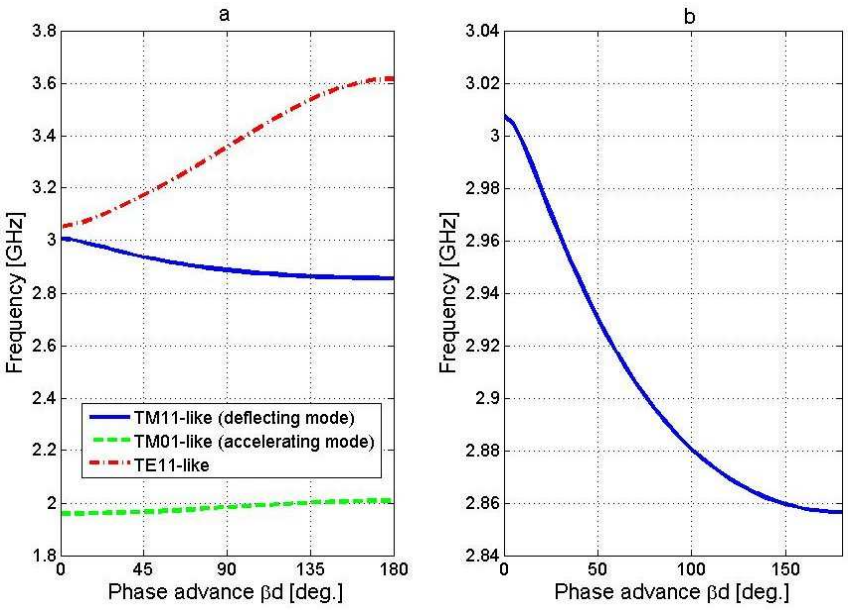

Fig. 14: (a) single cell dispersion curves; (b) detail of the deflecting mode dispersion curve (MAFIA results).

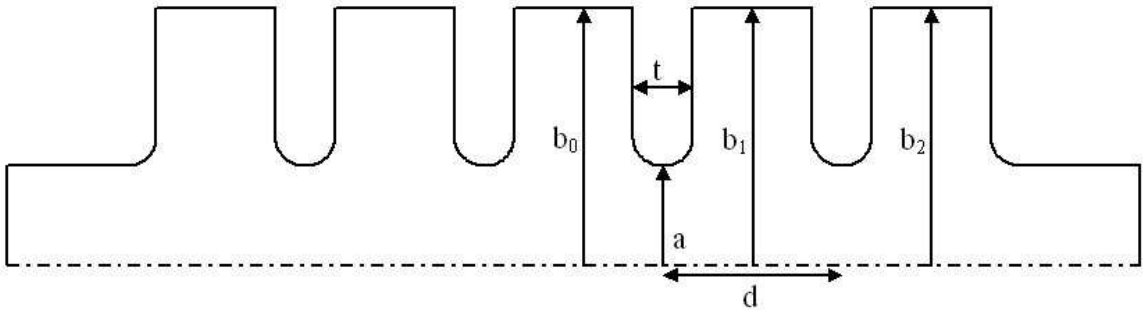

Fig. 15: 2D profile of the 5-cells deflecting structure.

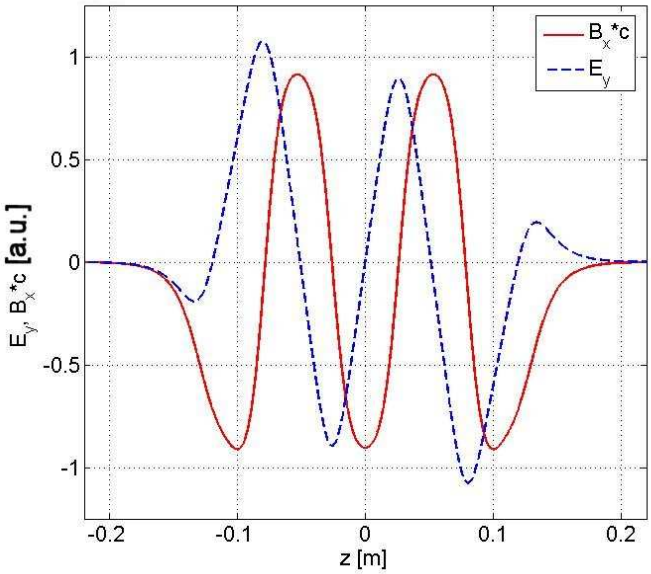

Fig. 16: B and E field of the 5-cells cavity obtained by MAFIA 2D.

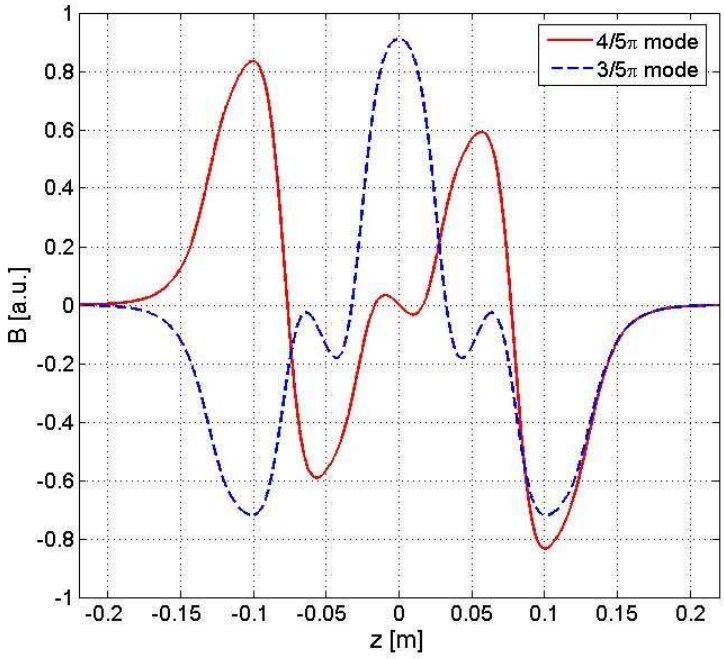

Fig. 17: B field profiles of the $4\pi/5$ mode and $3\pi/5$ modes.

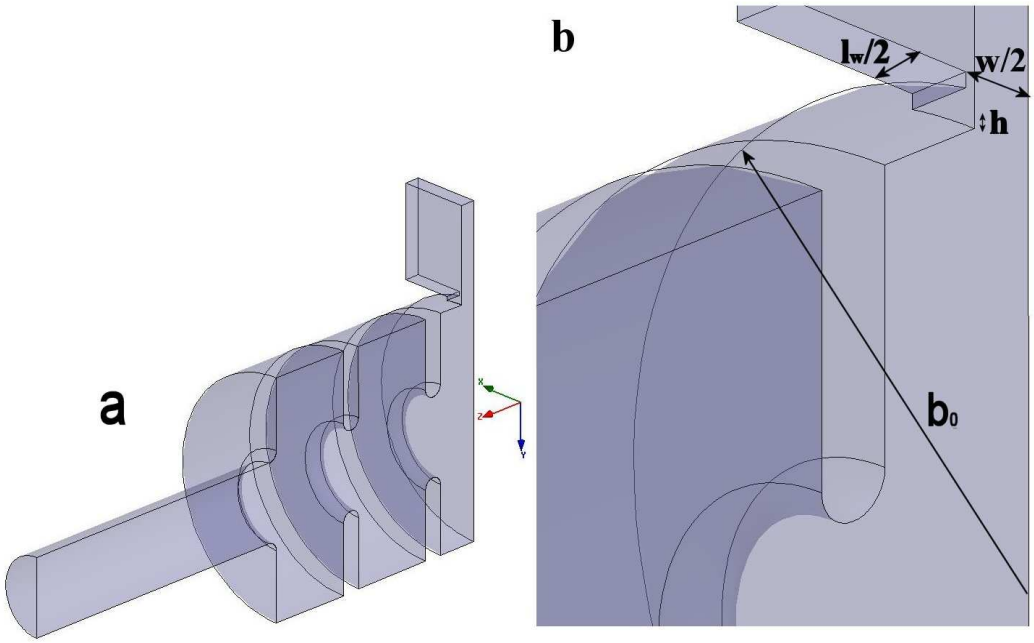

Fig. 18: 3D HFSS simulated structure with coupler.

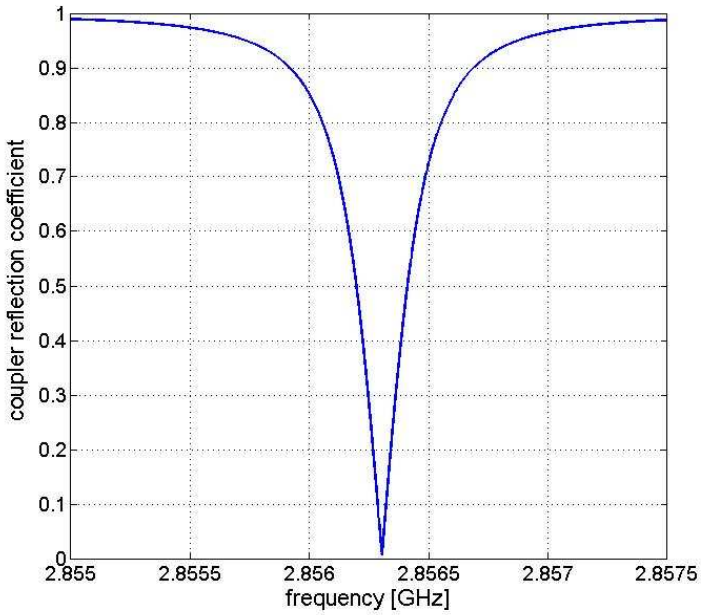

Fig. 19: Reflection coefficient at the input port obtained with HFSS.

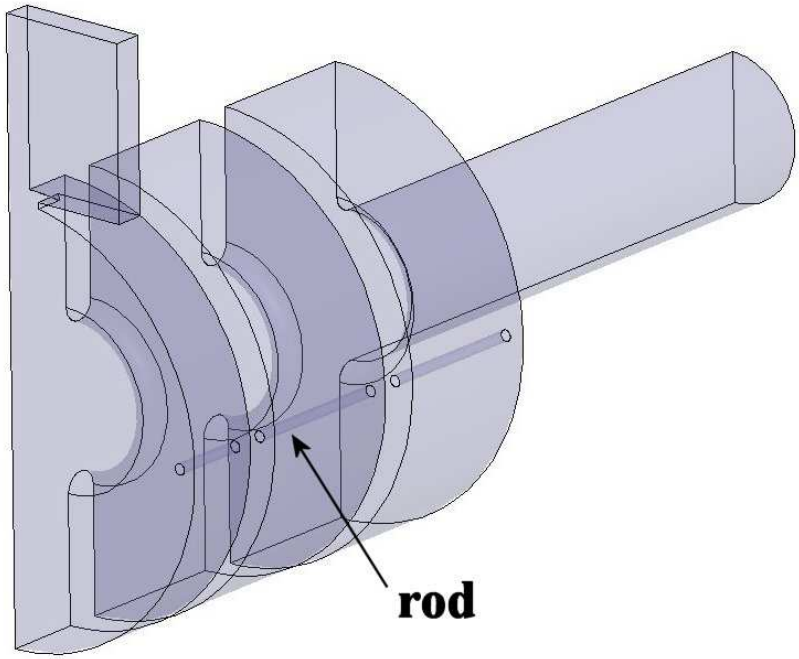

Fig. 20: Longitudinal rods to split the 90 deg tilted polarity.

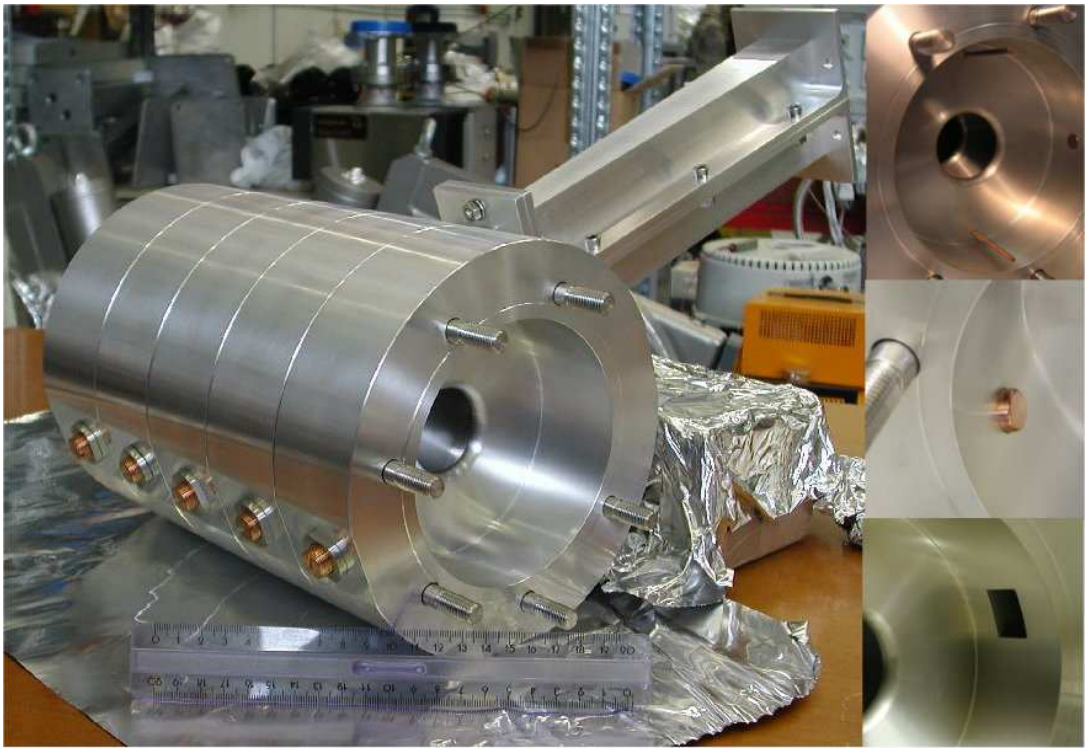

Fig 21: Deflector aluminum prototype and details of the coupling window, tuning system and rods.

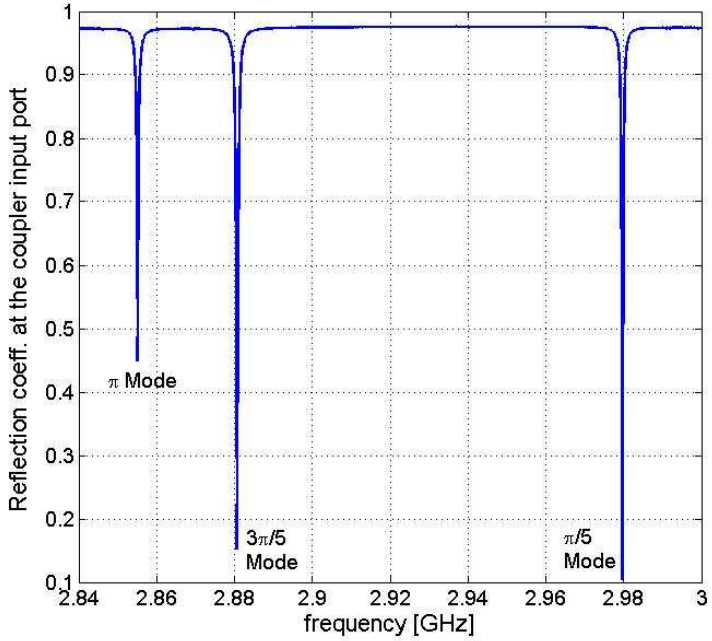

Fig. 22: measured reflection coefficient at the input coupler port.

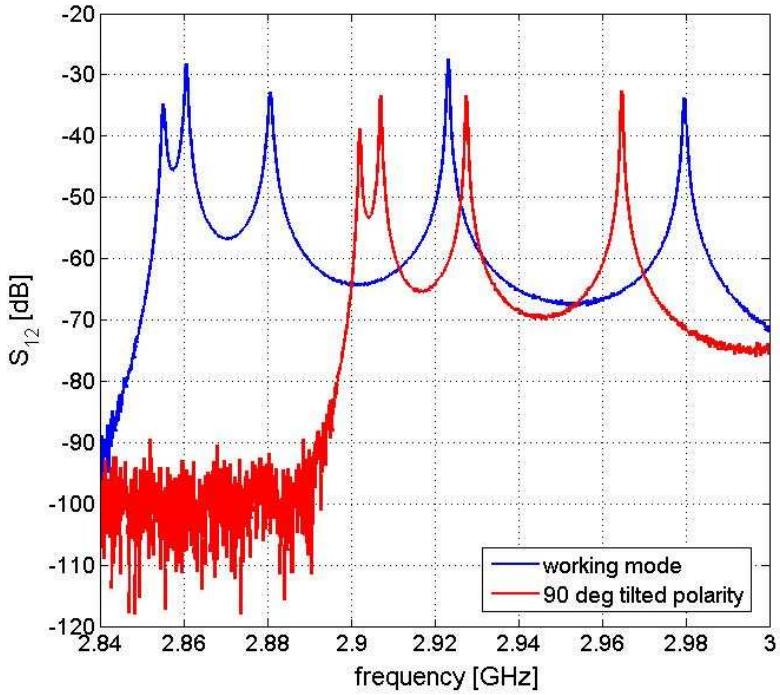

Fig. 23: transmission coefficient between the two antenna coupled with the working mode and between the two antenna coupled with the 90 deg tilted polarity.

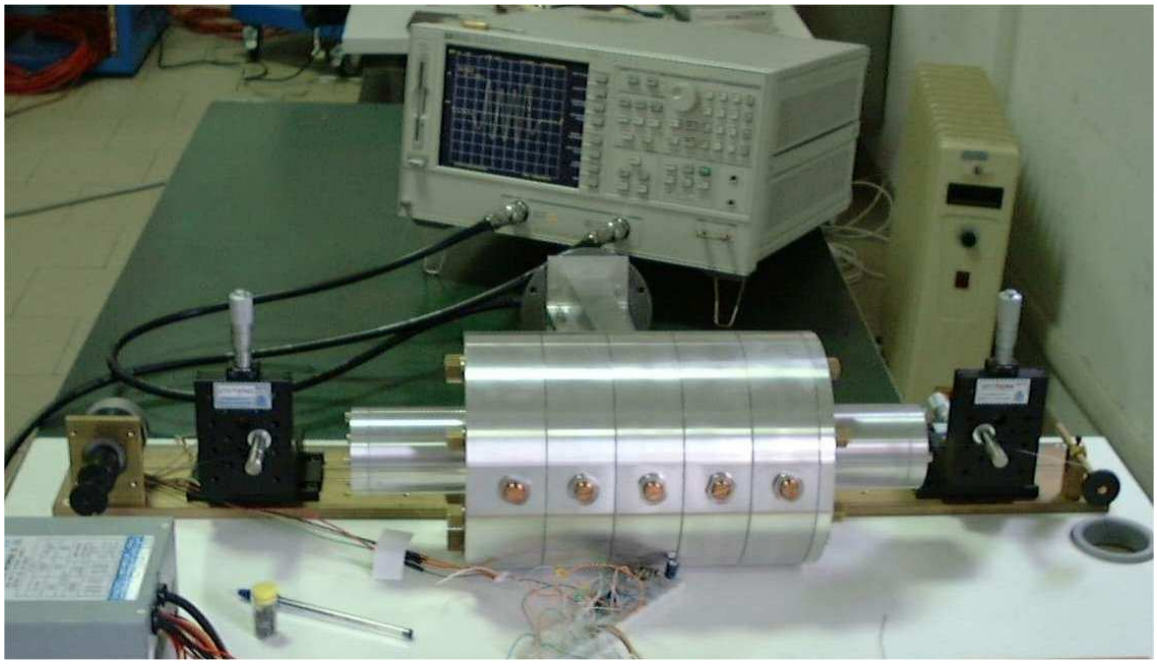

Fig. 24: bead-pull measurements setup.

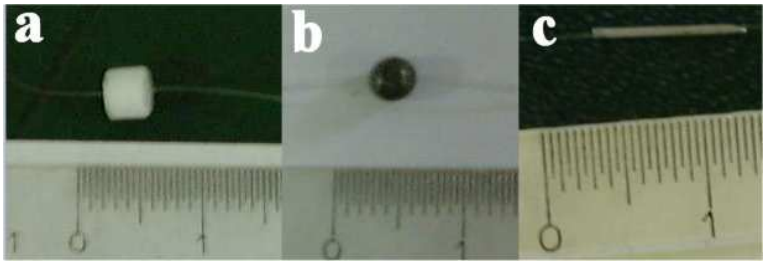

Fig 25: used perturbing objects: (a) dielectric cylinder; (b) metallic sphere; (c) metallic needle.

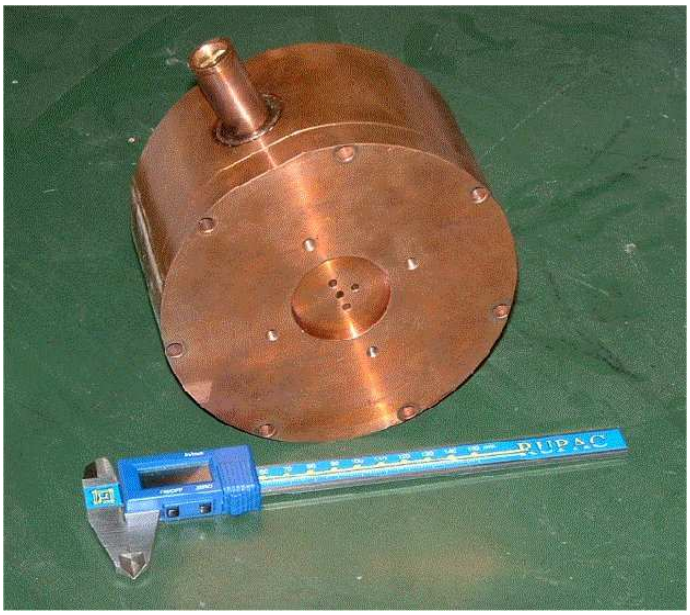

Fig. 26: pillbox cavity used for calibration of perturbing objects.

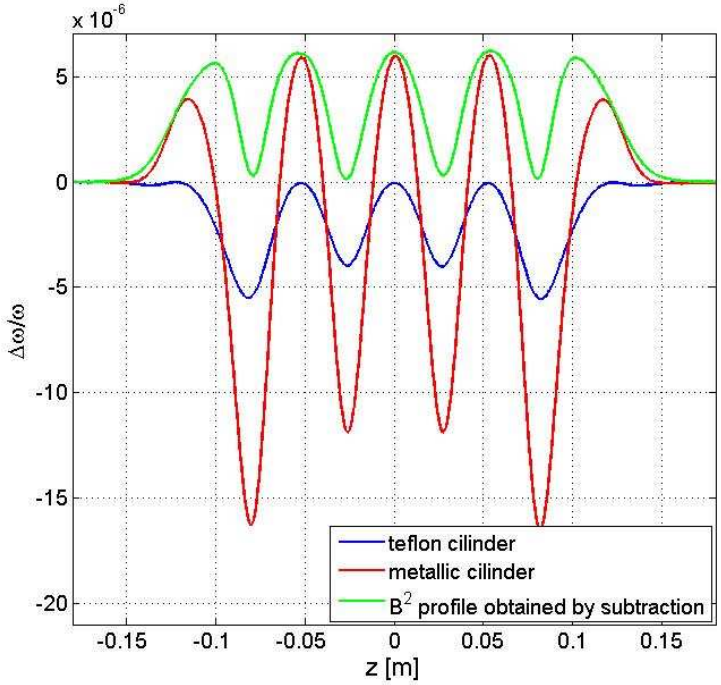

Fig. 27: results of the measurements using the metallic and the dielectric cylinder: average curves calculated over 30 measurements and B field profile calculated by subtraction.

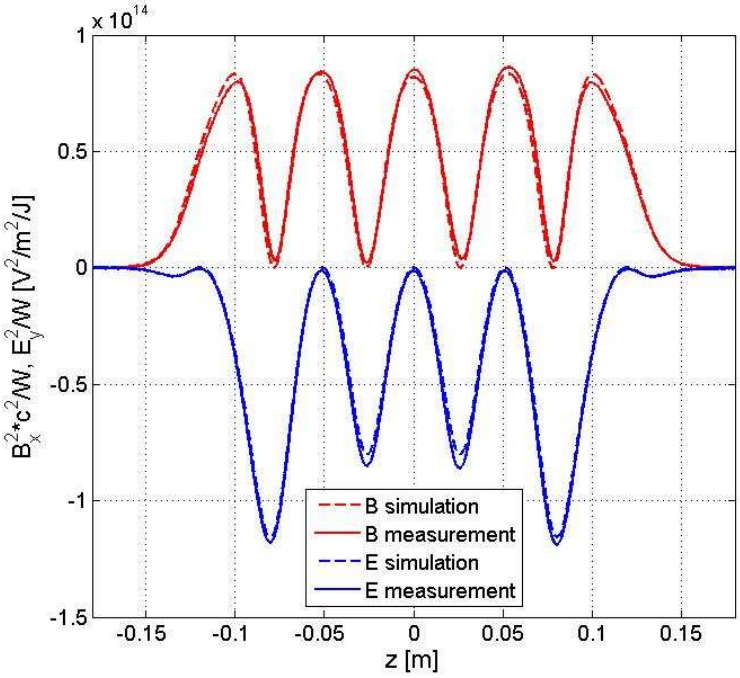

-ey

Fig. 28: B and E field components obtained calibrating the measurements with the form factor and comparison with simulation results obtained by MAFIA.

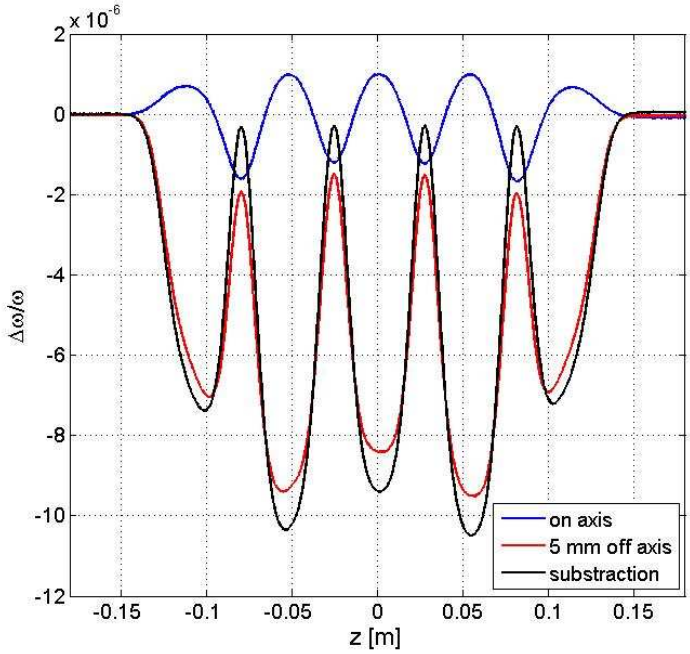

Fig. 29: measurement results obtained with a metallic needle on-axis and 5 mm off-axis. The longitudinal electric field component off-axis has been obtained by simply subtracting the two measurements.

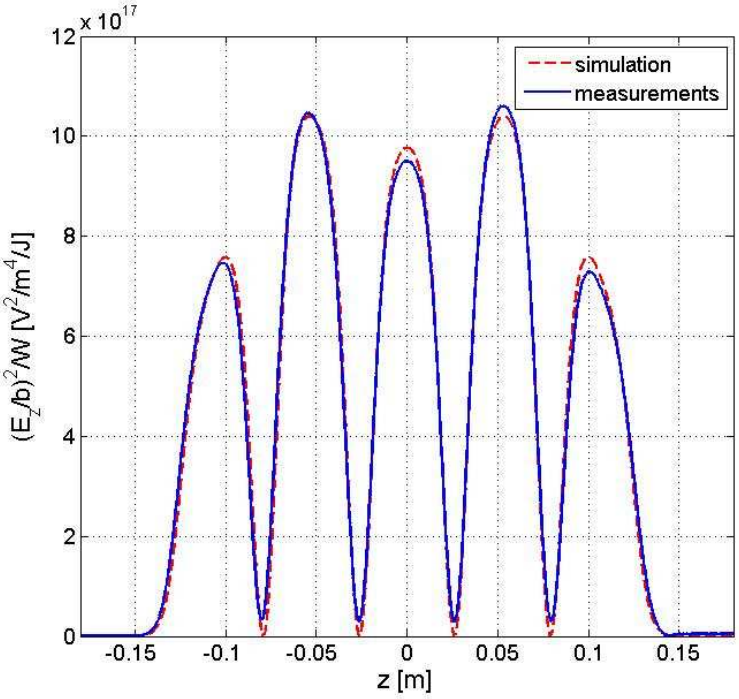

Fig. 30: longitudinal E field component normalized to the bead displacement from the axis b and comparison with simulation results obtained by MAFIA.

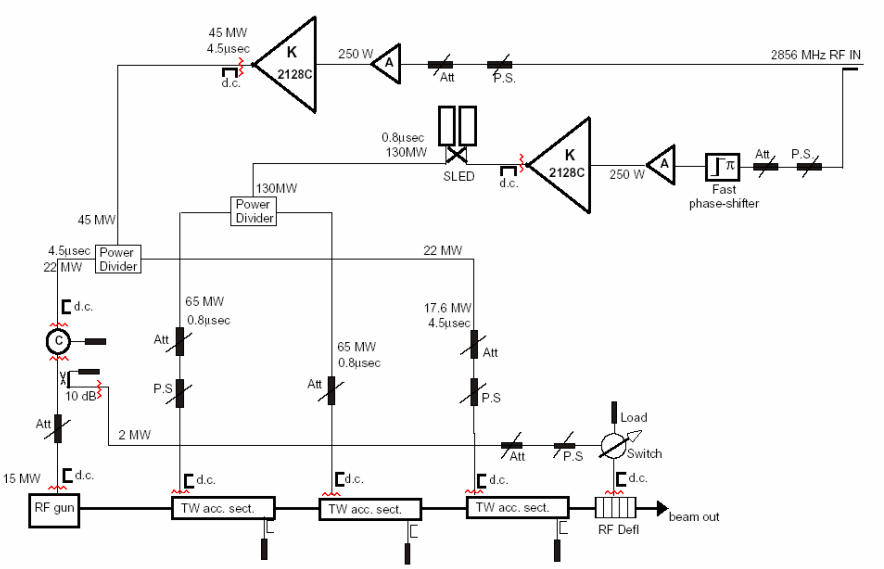

Fig. 31: Sketch of the RF deflector power feed system.